Quantum oscillations of magnetostriction and magnetic moment of tin under magnetic interaction conditions

V. M. Pudalov and M. S. Khaĭkin

Institute of Physics Problems, USSR Academy of Sciences
(Submitted July 4, 1974)
Zh. Eksp. Teor. Fiz. **67**, 2260–2279 (December 1974)

A method is proposed and realized which permits one to measure simultaneously oscillations of the magnetostriction u_{ik} and of the magnetic moment M. With the aid of the method one can determine the derivatives of the extremal area of the Fermi surface cross section from the components of the deformation tensor. The method is based on the fact that if $4\pi|\partial M/\partial H| \sim 1$ then the waveform of the u_{ik} oscillations contains information on the amplitude of M. The sepctrum of the M and u_{ik} oscillations is calculated. The effect of magnetic breakdown on the oscillations spectrum is considered. In this case from an analysis of the waveform of u_{ik}, one can also determine the dependence of the breakdown field on the lattice deformation. Oscillations of u_{ik} of tin are measured at $T = 0.37°K$, $H \sim 10^3$–10^4 Oe and $4\pi/|\partial M/\partial H| \approx 0.3$. A computer analysis of the waveform of the u_{ik} oscillations by means of the formulas derived in the paper yielded the absolute value of the M oscillations, a number of parameters that define this absolute value, and also the dependences of the extremal areas of the Fermi surface cross sections and of the breakdown field strength on the deformation-tensor components. Thus the presented method yields a new set of constants of the energy spectrum of metals, which can be used for testing and improving the theoretical calculations of the spectra.

I. INTRODUCTION

As is well known, variation of the magnetic field H gives rise to an oscillatory dependence of the dimensions of single crystals of metal; the nature of this dependence, in analogy with the oscillations of the magnetic moment M in the de Haas–van Alphen effect, is connected with Landau quantization. In the absence of magnetic interaction ($4\pi|\partial M/\partial H| \ll 1$) the components of the strain tensor u_{ik}, which describe this phenomenon, are determined by the thermodynamic relation [1]

$$u_{ik} = -\frac{\partial}{\partial \sigma_{ik}}\frac{\Phi}{V}. \qquad (1)$$

Here Φ/V is the thermodynamic potential per unit volume. Retaining in (1) the oscillatory part $\Phi \approx \Phi' \cos(\omega/H)$ [2], we obtain an expression for the oscillations of u_{ik}:

$$u_{ik} \approx 2\pi n \frac{\partial \ln \omega}{\partial \sigma_{ik}}\frac{\Phi'}{V}\sin\frac{\omega}{H} - \frac{\partial \ln \Phi'}{\partial \sigma_{ik}}\frac{\Phi'}{V}\cos\frac{\omega}{H} + \frac{\partial \ln V}{\partial \sigma_{ik}}\frac{\Phi'}{V}\cos\frac{\omega}{H}, \qquad (1')$$

where $n = \omega/2\pi H$ is the number of the oscillations in the reciprocal field. Since $\partial \ln V/\partial \sigma_{ik} = s_{llik}$, and

$$\frac{\partial \ln \omega}{\partial \sigma_{ik}} = \frac{\partial \ln \omega}{\partial u_{ll}}\frac{\partial u_{ll}}{\partial \sigma_{ik}} \sim s_{llik}$$

(s_{ijkl} is the inverse of the elasticity tensor c_{ijkl}), the ratio of the first term in (y′) to the third is $2\pi n$.

Under quasiclassical conditions, this is a large number. In particular, in our experiments $2\pi n \sim 10^3$ to 10^4. The second term in (1′) must be taken into account only in the quantum case ($n \sim 1$), or else if the derivative of any argument of Φ with respect to σ_{ik} is anomalously large. The latter situation is possible if, for example, lattice deformation changes the topology of the Fermi surface (FS) or lifts the degeneracy due to the crystal symmetry. In connection with magnetic breakdown, this case is considered in Sec. III. In the absence of such anomalies, we obtain from (1′) the relation

$$u_{ik} = -\frac{\partial \ln S}{\partial \sigma_{ik}} MH. \qquad (1'')$$

Here S is the extremal cross section of the FS. Thus, according to (1″), an investigation of the magnetostriction makes it possible to measure the tensor $\partial \ln S/\partial \sigma_{ik}$, knowledge of which is apparently just as important in the study of the electronic properties of metals as, for example, knowledge of the effective masses of the carriers

$$m^* = \mu m_e = \frac{1}{2\pi}\left(\frac{\partial S}{\partial \varepsilon}\right).$$

To obtain quantitative results, however, it is necessary to know besides u_{ik} also the absolute value of M. The known experimental methods for its determination are either insufficiently accurate [3] or complicated [4,5], so that both M and u_{ik} cannot be measured in a single experiment. Measurement of u_{ik} and M in different experiments [5], and all the more on different samples [6], lowers the reliability of the results.

The theory of Lifshitz and Kosevich [2] can serve as a basis for the calculation of the amplitude of the oscillations of the magnetic moment, if the curvature $\partial^2 S/\partial k_0^2$ of the FS cross section is known ($\hbar k_z$ is the momentum in the direction of the field **H**). At the present time this quantity can be determined only for certain FS sections in a few metals [3,4]. As to tin, the existing theoretical calculations of the FS [7,8] and the aggregate of the experimental data on the anisotropy of the de Haas–van Alphen effect [8,9] and the size effect [10] do not make it possible to establish even the order of magnitude of $\partial^2 S/\partial k_z^2$ for the small FS sections that determine the oscillatory dependence of u_{ik} in fields 10^3–10^4 Oe. At the same time, it is precisely these sections of the FS which are most sensitive to the parameters of the theoretical models, and this is the cause for the increased interest in their investigation.

There exists, however, one more possibility of determining M. It is connected with the fact that the contribution of the oscillations of M to the induction B in the sample, which is responsible for the formation of the quasiparticle energy levels, becomes appreciable at $4\pi|\partial M/\partial H| \sim 1$. The nonlinearity of this phenomenon complicates the spectrum of the oscillations. The amplitude of the new spectral components is determined by the value of M, and consequently the absolute value of M can

be determined from the ratio of the spectral components. The present paper contains an analysis and a realization of this method. In Sec. II, we calculate the spectrum of the u_{ik} oscillations, in Sec. III we consider the influence of magnetic breakdown on the u_{ik} spectrum, Sec. IV describes the experimental measurements, while in Secs. V and VI the calculations are compared with the experimental results.

II. CALCULATIONS OF THE u_{ik} OSCILLATION SPECTRUM

At $4\pi|\partial M/\partial H| \lesssim 1$, the magnetic moment of an ellipsoidal sample can be uniquely determined by solving the nonlinear equation [11]

$$M=\sum_{\nu}\sum_{r=1}^{\infty} {}^{\nu}A_r \sin\left[\left(\frac{\omega_\nu}{H+4\pi(1-D)M}-2\pi\gamma\right)r+\varphi_\nu\right], \qquad (2)$$

obtained by replacing the magnetic field intensity H in the Lifshitz-Kosevich formula [2] by its induction

$$B=H+4\pi(1-D)M. \qquad (3)$$

Here D is the demagnetizing factor, $\omega_\nu = cS_\nu/e\hbar$ is the circular frequency of the oscillations,

$$ {}^{\nu}A_r=-2k_B T\left(\frac{e}{ch}\right)^{3/2}\frac{\omega_\nu}{H^{1/2}}\left|\frac{\partial^2 S_\nu}{\partial k_z^2}\right|^{-1/2}\exp\left(-\frac{2\pi^2 r k_B {}^{\nu}T_D}{\hbar^{\nu}\omega_c}\right)$$

$$\times \mathrm{sh}^{-1}\left(-\frac{2\pi^2 r k_B T}{\hbar^{\nu}\omega_c}\right)\frac{1}{r^{1/2}}\cos\left(r\frac{\pi}{2}g_\nu\mu_\nu\right) \qquad (4)$$

is the amplitude of the r-th harmonic, g_ν is the g-factor averaged for the cross section ν, $\gamma = 1/2$ in the quasiclassical approximation for the trajectory without self-intersection and stopping points, $\varphi_\nu = \mathrm{sign}(\partial^2 S_\nu/\partial k_z^2)\pi/4$, $\hbar^{\nu}\omega_c = e\hbar H/\mu_\nu m_e c$ is the distance between the Landau levels, and the sum over ν means summation over all the extremal sections of the FS in the H direction.

Under real conditions we always have $|4\pi M/H| \ll 1$, and Eq. (2) can be simplified [11,12]:

$$M=\sum_{\nu}\sum_{r} {}^{\nu}A_r \sin[(\alpha_\nu - K_\nu M)r+\varphi_\nu], \qquad (5)$$

$$K_\nu = 4\pi(1-D)\omega_\nu/H^2, \quad \alpha_\nu=\omega_\nu/H-2\pi\gamma.$$

An exact solution of (5) was obtained by Shoenberg [12] at r = 1 and ν = 1, 2. In the general case, Eq. (5) can be solved with any degree of accuracy by successive approximations, as was proposed by Phillips and Gold [3]. The solution is a series containing different powers and products of ${}^{\nu}A_r$ for harmonic functions of all possible combination frequencies $\tilde{\omega}_j$. Since ${}^{\nu}A_1$ in (4) is determined to a considerable degree by the exponential factor $\sim \exp[-2\pi^2 k_B(T+T_D)/\hbar\omega_c]$, it is convenient to classify the terms of the series in accordance to powers of its factor q:

$$M=\sum_j \tilde{M}_j \sin(\tilde{\omega}_j/H+\tilde{\varphi}_j),$$

$$\tilde{\omega}_j/H+\tilde{\varphi}_j=\sum_r\sum_\nu (r\alpha_\nu+\varphi_\nu){}^{\nu}n_r. \qquad (6)$$

Here ${}^{\nu}n_r$ are arbitrary integers, and

$$\sum_{r,\nu} r|{}^{\nu}n_r| = q.$$

At $|K_\nu^\nu A_1| < 1$, the series (6) converges like $(K_\nu^\nu A_1)^q$. Table I lists the coefficients of the terms of the series (6) up to $o(KA)^3$ for the case of two extremal cross sections S_1 and S_2.

We expand u_{ik} in a series in the functions (6):

$$u_{ik}=\sum_j \tilde{u}_{ik}^{(j)}\sin(\tilde{\omega}_j/H+\tilde{\varphi}_j). \qquad (7)$$

It is clear that for each combination frequency $\tilde{\omega}_j = n\omega_1 + m\omega_2$, we have the following relation, which follows from (1″):

$$\tilde{u}_{ik}^{(j)}=-\frac{\partial\tilde{\omega}_j}{\tilde{\omega}_j\,\partial\sigma_{ik}}H\tilde{M}_j=-\left(n\frac{\partial\ln S_1}{\partial\sigma_{ik}}\frac{\omega_1}{\tilde{\omega}_j}+m\frac{\partial\ln S_2}{\partial\sigma_{ik}}\frac{\omega_2}{\tilde{\omega}_j}\right)H\tilde{M}_j. \qquad (8)$$

The expansion (7), (8) of the experimentally measured quantity u_{ik} in terms of the functions of Table I enables us to find the absolute value of the angular momentum (or $\partial \ln S/\partial\sigma_{ik}$):

$$\frac{\tilde{u}_{ik}^{(2)}}{\tilde{u}_{ik}^{(1)}}=\frac{\tilde{M}_2}{\tilde{M}_1}=-\frac{1}{2}K_1\tilde{M}_1+o(K_1{}^1A_1)^2,$$

$$\frac{(\tilde{u}_{ik}^{(1)})^2}{\tilde{u}_{ik}^{(2)}}=\frac{\partial\ln S_1}{\partial\sigma_{ik}}\frac{-2}{K_1}+o(K_1{}^1A_1)^2. \qquad (9)$$

III. EFFECT OF MAGNETIC BREAKDOWN ON THE u_{ik} OSCILLATION SPECTRUM

Having in mind the performed experiments, let us consider the case when one of the extremal sections, for example ν = 1, experiences the two points of the trajectory an interband magnetic breakdown. An expression for the oscillations of the thermodynamic potential Φ in the presence of breakdown was found by Kochkin [13] and takes the following form for simple non-combinatorial cross sections (n = −k in the notation of [13])[1)]

$${}^{1}\Phi=\sum_{r=1}^{\infty} {}^{1}\Phi_r \cos\left[\left(\frac{\omega_1}{H}-2\pi\gamma-2\Omega\right)r+\varphi_1\right]. \qquad (10)$$

Here

$${}^{1}\Phi_r=-\frac{H^2}{\omega_1}\frac{1}{r}{}^{1}A_r\tau^{2r}, \qquad (11)$$

$\tau^2 = 1 - \exp(-H_0/H)$ is the probability of remaining in the same band, H_0 is the characteristic breakdown field, and Ω is a monotonic function of the field ($\Omega \to 0$ as $H \to 0$ and $\Omega \to -\pi/4$ as $H \to \infty$). Allowance for the magnetic interaction in (10) reduces, in analogy with (2), to replacing H in the arguments of the oscillating functions by the magnetic field induction B [Eq. (3)]. M is given by formula (6) and Table I, where it is now necessary to make the obvious substitution

$${}^{1}A_r \to {}^{1}A_r\tau^{2r}, \quad \alpha_1 \to \alpha_1 - 2\Omega. \qquad (12)$$

Formulas (7) and (8), as before, make it possible to find that part of the strain tensor u_{ik} which is connected with

TABLE I. Coefficients $\tilde{M}_j$ of the expansion of the magnetic moment (6)

j	Argument of function	q = 1	q = 2	q = 3
1	$\alpha_1+\varphi_1$	${}^{1}A_1$		$-K_1{}^2{}^{1}A_1({}^{1}A_1{}^2+2\,{}^{2}A_1{}^2)/8$
2	$2\alpha_1+2\varphi_1$		$-K_1{}^{1}A_1{}^2/2$	
3	$2\alpha_1+\varphi_1$		${}^{1}A_2$	
4	$3\alpha_1+3\varphi_1$			$3K_1{}^2{}^{1}A_1{}^3/8$
5	$3\alpha_1+2\varphi_1$			$-3K_1{}^{1}A_1{}^{1}A_2/2$
6	$3\alpha_1+\varphi_1$			${}^{1}A_3$
7	α_1			$K_1{}^{1}A_1{}^{1}A_2/2$
8	$2\alpha_1+\alpha_2+2\varphi_1+\varphi_2$			$(2K_1+K_2)^2{}^{1}A_1{}^2{}^{2}A_1/8$
9	$2\alpha_1+\alpha_2+\varphi_1+\varphi_2$			$-(2K_1+K_2){}^{1}A_2{}^2A_1/2$
10	$2\alpha_1-\alpha_2+2\varphi_1-\varphi_2$			$-(2K_1-K_2)^2{}^{1}A_1{}^2{}^{2}A_1/8$
11	$2\alpha_1-\alpha_2+\varphi_1-\varphi_2$			$(2K_1-K_2){}^{1}A_2{}^2A_1/8$
12	$\alpha_1+\alpha_2+\varphi_1+\varphi_2$		$-(K_1+K_2){}^{1}A_1{}^2A_1/2$	
13	$\alpha_2-\alpha_1+\varphi_2-\varphi_1$		$(K_2-K_1){}^{1}A_1{}^2A_1/2$	

Note. The lines j = 14 to 24 are obtained from the first 11 lines by making the substitutions

$$\begin{pmatrix} \varphi_1\to\varphi_2 \\ \alpha_1\to\alpha_2 \\ K_1\to K_2 \\ {}^{1}A_r\to{}^{2}A_r \\ j\to 25-j \end{pmatrix}$$

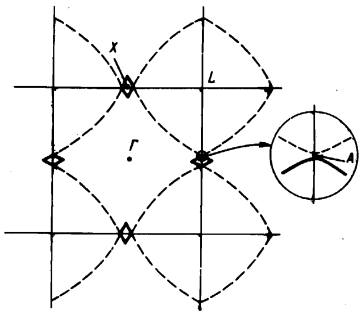

FIG. 1. Contours of the intersection with the (001) plane: thin solid lines—Brillouin zones, thick lines—FS in zone III (orbit δ_1^1), dashed line—FS in zone IV.

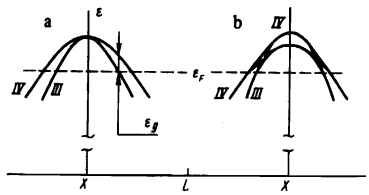

FIG. 2. Schematic representation of two branches of the band structure of tin on the XL line: a) in nondeformed lattice, b) in the case of deformation that lifts the degeneracy.

the dependence of the areas of the Fermi surface on σ_{ik}:

$$ {}^{I}u_{ik} = -\sum_j \frac{\partial \tilde{\omega}_j}{\tilde{\omega}_j \partial \sigma_{ik}} H \tilde{M}_j. \qquad (13) $$

We shall show, with the concrete situation of magnetic breakdown in tin between zones III and IV as an example [9], how it becomes necessary to take the terms of the type of the second term of (1′) into account. Figure 1 shows the contours of the intersection between the basal plane and two closely-lying sections of the FS, while Fig. 2a shows schematically the two corresponding branches of the $\epsilon(k)$ spectrum [7]. In the absence of spin-orbit interaction, both branches coincide along the line XL, which is the intersection of the face of the Brillouin zone [14], the (001) plane containing the points Γ, X, and L (Fig. 1). The FS intersection contours in zones III and IV has a common point (A in Fig. 1) on the intersection of the arcs corresponding to the pieces of the free-electron sphere. The spin-orbit interaction lifts this obligatory degeneracy in all points of the XL line, with the exception of the point X. Thus, the trajectories in Fig. 1 are separated at the point A by δk, while the branches of the spectrum in Fig. 2a are separated by $\epsilon_g(A) = \Delta$. The double degeneracy at the point X is due to the fact that the symmetry group of the vector ΓX contains the twofold axis [110]. [14] Consequently, the strain u_{11} in the basal plane lifts the degeneracy at the point X, and by expanding ϵ_g in a series in the small deformation u we get

$$ \varepsilon_g = \Delta + u(\partial\Delta/\partial u + \partial\varepsilon_x/\partial u). $$

Since $\partial\Delta/\partial u \sim \Delta$, $\partial\epsilon_x/\partial u \sim \epsilon_F$, and $H_0 \sim (\epsilon_g)^2/\epsilon_F\mu_B$, it follows that $\partial \ln H_0/\partial u \sim 2\partial \ln \epsilon_g/\partial u \sim \epsilon_F/\epsilon_g \sim 10^3$. Here μ_B is the Bohr magneton and ϵ_F is the Fermi surface. From the foregoing estimate it is seen that $\partial \ln H_0/\partial u \sim 2\pi n$, and the second term in (1′) becomes comparable in magnitude with the first.

After substituting (3) in (10) we can expand ${}^1\Phi$, in accordance with the scheme described above, in a series in the functions of the restructured spectrum:

$$ {}^1\Phi = \sum_j {}^1\tilde{\Phi}_j \cos(\tilde{\omega}_j/H + \tilde{\varphi}_j), $$

$$ \tilde{\omega}_j/H + \tilde{\varphi}_j = \sum_r \sum_\nu (r\alpha_\nu + \varphi_\nu)^\nu n_r. \qquad (14) $$

Table II lists the nonvanishing coefficients ${}^1\tilde{\Phi}_j$ up to $o(KA)^3$ for the case of two extremal sections $\nu = 1$ and 2, and magnetic breakdown for $\nu = 1$. Unlike in Table I, ${}^1A_r$ and α_1 take the form (12). The corresponding part of the strain tensor, which is connected with the dependence of the breakdown field on σ_{ik}, is obtained from (1′), (10) and (11):

$$ {}^{II}u_{ik} = -\frac{\partial \ln H_0}{\partial \sigma_{ik}} \frac{H_0}{H} s^2 \sum_j \frac{\partial {}^1\tilde{\Phi}_j}{\partial(\tau^2)}; \qquad (15) $$

Here $s^2 = (1 - \tau^2)$ is the breakdown probability.

Summing the contributions of (13) and (15), we obtain the complete expression for the u_{ik} oscillations in the presence of magnetic breakdown:

$$ u_{ik} = {}^{I}u_{ik} + {}^{II}u_{ik}. $$

These two parts of the strain tensor have different phases of the oscillating functions and different dependences of the amplitude on the magnetic field. Thus,

$$ |{}^{II}u_{ik}/{}^{I}u_{ik}| \to 0 \quad \text{as} \quad H \to 0, $$

$$ |{}^{II}u_{ik}/{}^{I}u_{ik}| \to \infty \quad \text{as} \quad H \to \infty. $$

This circumstance enables us, in the analysis of the amplitude and waveform of the oscillations of u_{ik}, to separate the contributions of the two terms and by the same token determine the dependence of the breakdown field on the components of the strain tensor.

As seen from Table II and formula (4), the initial phases and the dependence of the amplitude on the field and on the temperature are different for the terms of the series (7), which result from the magnetic interaction, and for the usual harmonics [2] of the same frequency. This circumstance, and also the appearance in the spectrum of combination frequencies that result only from the magnetic interaction, enable us, by analyzing the waveform of the oscillations of u_{ik} at different H and T, to determine all the parameters that enter in the phenomenological theory [2]:

$$ T_D,\ \mu,\ g,\ \partial^2 S/\partial k_z^2,\ \partial \ln S/\partial \sigma_{ik}. \qquad (16) $$

The first two of them, just as in the case $4\pi|\partial M/\partial H| \ll 1$, determine in the main the dependence of the amplitude of the oscillations on H and T. The g factor has been determined from a harmonic analysis of the oscilla-

TABLE II. Coefficients $\tilde{\Phi}_j$ of the expansion of the thermodynamic potential (14).

j	Argument of the function (12)	q = 1	q = 2	q = 3
1	$\alpha_1 + \varphi_1$	${}^1\Phi_1$		$-K_1{}^2{}^1\Phi_1(3\,{}^1A_1{}^2 + 2\,{}^2A_1{}^2)/8$
2	$2\alpha_1 + 2\varphi_1$		$-K_1\,{}^1\Phi_1\,{}^1A_1/2$	
3	$2\alpha_1 + \varphi_1$		${}^1\Phi_2$	
4	$3\alpha_1 + 3\varphi_1$			$3K^2{}_1\,{}^1\Phi_1\,{}^1A_1{}^2/8$
5	$3\alpha_1 + 2\varphi_1$			$-K_1({}^1\Phi_1\,{}^1A_2 + {}^1\Phi_2\,{}^1A_1)/2$
6	$3\alpha_1 + \varphi_1$			${}^1\Phi_3$
7	α_1			$K_1({}^1\Phi_2\,{}^1A_1 + {}^1\Phi_1\,{}^1A_2)/2$
8	$2\alpha_1 + \alpha_2 + 2\varphi_1 + \varphi_2$			$K_1(K_1 + K_2)\,{}^1\Phi_1\,{}^1A_1{}^2A_1/4$
9	$2\alpha_1 + \alpha_2 + \varphi_1 + \varphi_2$			$-K_1\,{}^1\Phi_2{}^2A_1/2$
10	$2\alpha_1 - \alpha_2 + 2\varphi_1 - \varphi_2$			$-K_1(2K_1 - K_2)\,{}^1\Phi_1\,{}^1A_1\,{}^2A_1/4$
11	$2\alpha_1 - \alpha_2 + \varphi_1 - \varphi_2$			$K_1\,{}^1\Phi_2{}^2A_1/2$
12	$\alpha_1 + \alpha_2 + \varphi_1 + \varphi_2$		$-K_1\,{}^1\Phi_1\,{}^2A_1/2$	
13	$\alpha_2 - \alpha_1 + \varphi_2 - \varphi_1$		$K_1\,{}^1\Phi_1\,{}^2A_1/2$	
14	$2\alpha_2 - \alpha_1 + \varphi_2 - \varphi_1$			$K_1\,{}^1\Phi_1\,{}^2A_2/2$
15	$2\alpha_2 - \alpha_1 + 2\varphi_2 - \varphi_1$			$-K_1(2K_2 - K_1)\,{}^1\Phi_1\,{}^2A_1{}^2/8$
16	$2\alpha_2 + \alpha_1 + \varphi_2 + \varphi_1$			$-K_1\,{}^1\Phi_1\,{}^2A_2/2$
17	$2\alpha_2 + \alpha_1 + 2\varphi_2 + \varphi_1$			$K_1(2K_2 + K_1)\,{}^1\Phi_1\,{}^2A_1{}^2/8$
18	$\alpha_2 + \varphi_2$			$-K_1K_2\,{}^1\Phi_1\,{}^1A_1\,{}^2A_1/2$

tions, for example, in [3,4], and the presence of magnetic interaction does not complicate this problem. As to the next to the last parameters in (16), the parameter $|\partial^2 S/\partial k_z^2|^{-1/2}$ is contained as a numerical factor in the amplitude of the oscillations in the theory of [2] and therefore cannot be determined from a harmonic analysis of the oscillations. Under the conditions of magnetic interaction, as seen from Table I, the multiplicativity of the parameters $\partial^2 S/\partial k_z^2$ and $\partial \ln S/\partial \sigma_{ik}$ no longer hold, and consequently they can be determined independently.

The accuracy with which the quantities $\partial \ln S/\partial \sigma_{ik}$, $\partial^2 S/\partial k_z^2$, $\partial \ln H_0/\partial \sigma_{ik}$, ..., can be determined by this method is proportional to $4\pi|\partial M/\partial H| \sim |KA|$, and to increase this accuracy it is necessary to decrease T and H, inasmuch as $KA \propto H^{-3/2}$ as $T/H \to 0$.

For a complete realization of the possibilities of the considered method and of the dilatometer resolution δu_{ik} it is rational to measure u_{ik} and reduce the data with the derived formulas in two stages. First it is necessary to perform the measurements in the range $\Delta H \sim H$ in order to establish the numbers of the oscillations, the sign of $\partial \ln S/\partial \sigma_{ik}$, and the quadrant of the argument $(\pi g\mu/2)$. Analysis of the oscillation waveform during this stage yields the final values of ω_ν, ${}^\nu T_D$, and μ_ν, as well as preliminary values of g_ν, $|\partial^2 S_\nu/\partial k_z^2|$, and $\partial \ln S_\nu/\partial \sigma_{ik}$. It is next necessary to measure the waveform of the oscillations with a higher field resolution in several sections of the interval ΔH. The reduction of the measurement data during this stage makes it possible to refine the values of g_ν, $\partial^2 S_\nu/\partial k_z^2$, and $\partial \ln S_\nu/\partial \sigma_{ik}$.

IV. EXPERIMENT

Since the purpose of the experiment was the exact measurement of the amplitude and waveform of the oscillations, it was necessary to use samples of ellipsoidal shape. The spherical shape of the sample made it possible, furthermore, to measure u_{ik} of one and the same sample in different directions.

The object of the experiment was chosen to be tin, for the following reasons:

1) The multiply-connected Fermi surface of tin has small sections that are very sensitive to lattice deformation, and this leads to a large amplitude of u_{ik}. Small sections of the Fermi surface play an important role in the comparison of the theory with experiment, since their shape is most sensitive to variations of the parameters of the theoretical models.

2) The relatively low melting temperature and purity of the initial material make it possible to obtain tin single crystals of high grade ($T_D \sim 10^{-2}$–10^{-1} °K) [15].

3) The influence of the magnetic interaction on the u_{ik} oscillations due to small sections of the Fermi surface of tin and on M becomes maximal already in a field $H \sim 10^3$–10^4 Oe (T = 0.37°K) [16].

To increase the signal/noise ratio it is customary in experiments to use the method of single slow scanning, for example, of the magnetic field and to perform the measurement with maximum time constant of the optimal filter. It is known, however, that it is more effective to use for this purpose the alternative method developed for NMR spectroscopy, namely multiple scanning with coherent summation of the results of each scanning, and accordingly, with smaller time constants of the optimal filter. To perform the coherent summation it is obviously necessary to use a multichannel storage unit. The optimal filter is customarily a modulation receiving circuit with synchronous detector.

The modulation receiving circuit is ill-suited for amplitude measurements, since the requirement that the modulation field be homogeneous in the sample volume makes it necessary to lower the modulation frequency, which then falls into the background noise region. The measurements were therefore performed by the method of multichannel storage, without modulating the magnetic field. The lower frequency of the pass band of the digital filter was then determined by the time of single scanning, while the upper frequency was determined by the counting time in one channel (or by the number of channels).

The sample. A spherical tin single crystal of 1 cm diameter was grown from the melt in a dismountable quartz mold by the method described in [17]. A thin channel ~20 mm long with cross section ~0.5 × 0.5 mm connected the spherical cavity of the mold with the cold end. When the mold is cooled with a temperature gradient, a single crystal grows in this channel, and serves subsequently as the primer for the crystallization of the sample. The sample grown in this manner was etched with dilute hydrochloric acid (~15%), and the directions of its crystallographic axes were determined from the etch figures. The error in the orientation of the sample in the dilatometer relative to the direction of the measurement of the striction was not more than 3°.

Measurement system. The measurements of u_{ik} were performed, in analogy with [15], with a dilatometer [18]. The sample was mechanically coupled to a thin membrane—the bottom of a resonator [18]. The change in the dimensions of the sample deforms the resonator and consequently produces a shift Δf of the frequency f of the 3-cm self-oscillator whose feedback circuit contains the resonator.

For convenience in the registration of Δf, the frequency of the measurement generator (MG) is shifted to the acoustic band via triple heterodyning (Fig. 3). The first heterodyne is a self-oscillator [19]. Two broadband amplifiers AI and AII served simultaneously as low-pass filters. The output audio signal of AII, of frequency $F = f - \Sigma_i f_i$, was fed to the input of the multichannel storage (MS) [20] (f_i is the frequency of the i-th heterodyne).

The turning-on of the next channel of the storage unit means the arrival of a pulse "+1" from the quartz clock to the input of the address register. Simultaneously, the

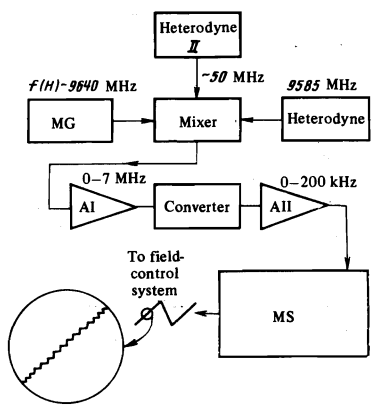

FIG. 3. Block diagram of the system for recording frequency deviation.

input gates open for a fixed time ΔT, and a number of pulses, equal to $F\Delta T$, enters the counting input of the register of the arithmetic unit. This number is then recorded in the memory in the address of the running state of the address register. The next channel is then turned on, and the cycle is repeated. After the last channel is reached, the address register is reversed. In the next accumulation, the newly arriving number of pulses is added to the pulses previously recorded in the same address. Connected in parallel to the address register is a code-voltage converter, the output of which is a sawtooth voltage consisting of 1024 (512, 256) steps. This voltage is used to control the magnetic field [21].

The magnetic field is scanned many times in one and the same band, in accord with the set-point voltage from the multichannel storage, and the results of the successive scannings are coherently summed in the memory unit. The signal amplitude is proportional here to N, the noise amplitude is proportional to $\sqrt{N}$, and the signal/noise ratio increases like $\sqrt{N}$ (Fig. 4). The dilatometer resolution is $\delta u_{ik} \sim 10^{-11}$, and the accuracy with which Δf is converted into u_{ik} is 2%.

Magnetic field. To study the waveform of the oscillations it is necessary to record without distortion the entire spectral region, whose width is determined, as seen from Table I, by the quantity $KA \approx 4\pi\partial M/\partial H$. The experiment was performed under conditions $KA \sim 0.1$. The higher harmonics and the spectrum of the oscillations of u_{ik} with amplitude $\gtrsim 0.5\%$ of the amplitude of the fundamental tone were contained in the range $(0-3)\omega_{1,2}$. Among the possible causes of the distortion of the oscillation waveform, the most significant are:

1) inhomogeneity of the field over the dimension of the sample;

2) shift of the successively summed results of the scanning relative to one another over the field ("incoherence");

3) the difference between the field in the sample and the field in the magnetic gap, due to eddy currents induced in the sample by the rapidly alternating magnetic field.

The field distortion due to causes 1)—3) can be much smaller than the minimum period in the spectrum:

$$\delta H/H \ll 2\pi H/3\omega_{1,2} \sim 5\cdot 10^{-4} \text{ (in 6-kOe field).}$$

The following conditions obtained in the experiment:

1) The inhomogeneity of the electromagnetic field, as determined from the NMR signal, did not exceed 10^{-4} over the sample dimension.

2) The field scanning system [21] ensured that there was no shift over the field at a 10^{-4} level as the initial scanning point was periodically readjusted against the NMR signal.

3) To determine the maximum permissible scanning rate, the results of two successive measurements performed with different velocity were subtracted from each other. It was established that at a scanning rate $\lesssim 10$ channels/sec (~ 10 Oe/sec in a field 6000 Oe), the difference signal obtained in this manner does not exceed the noise level.

The entire investigated magnetic-field interval, 4—9 kOe, was broken up into several bands 500—1000 Oe wide, and the field was scanned within the limits of one band. The 512-channel breakdown of the band has made it possible to register signals in a spectral region not narrower than $(0-4)\omega_{1,2}$. The direction of the magnetic field along the crystallographic axes was established, with accuracy $\sim 20'$, by the symmetry of the effect in two phases.

V. REDUCTION OF EXPERIMENTAL RESULTS

A. τ-Oscillations

With the magnetic field directed in the (001) plane, we observed oscillations of u_{11} and u_{33} [15], due to the small electronic part of the Fermi surface in zone VI. The measurements were performed in the field interval 4—9 kOe and in the temperature interval 0.37—1.3°K. At a magnetic field direction $\mathbf{H} \parallel [010]$, we registered beats of two neighboring frequencies (Fig. 5). The relative frequency difference decreased to 0.5% when the field was inclined away from the [010] axis through an angle $\sim 14°$ in the planes (100) and (001) (Fig. 6). These two observed frequencies can be naturally connected with the two extremal sections of the surface shown in Fig. 7.

1. u_{11}; $\mathbf{H} \parallel [010]$. The simultaneous determination of the mean-squared approximations of all the experimental points $u_{11}(H, T)$ from all the unknown parameters is an extremely slow problem calling for a tremendous memory ($\sim 10^5$ words). The measurements were therefore reduced in two stages. First, the dependence of the oscillation amplitude on the field and on the temperature was used to determine $^{1,2}T_D$ and $\mu_{1,2}$.[2)]

The totality of the measurements at T = 0.37°K (2550 points of $U_{11}(H)$) was then fed from a punched tape into a BÉSM-6 computer. This was followed by a least-

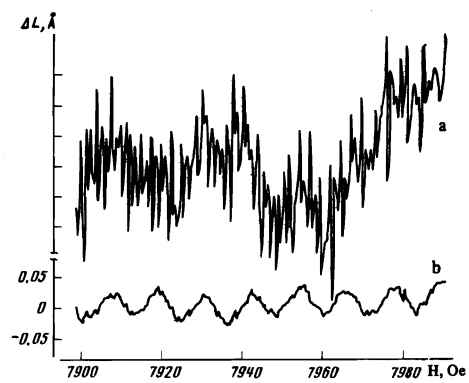

FIG. 4. Oscillations of $u_{33}(\tau^1)$; $\mathbf{H} \parallel [110]$, T = 0.37°K. a) Results of single scanning; b) improvement of the signal/noise ratio by 18 dB as a result of 64 scannings. Both curves are plotted in a single scale of ΔL.

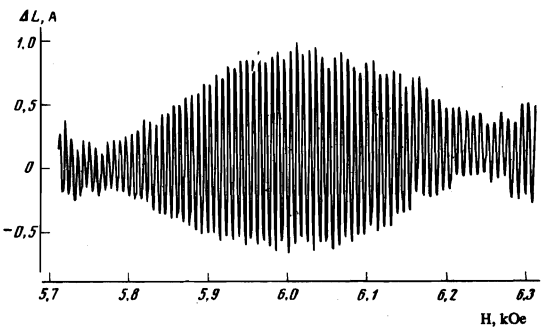

FIG. 5. Segment of the plot of the oscillations of $u_{11}(\tau^1, \tau^2)$; T = 0.37 K, $\mathbf{H} \parallel [010]$.

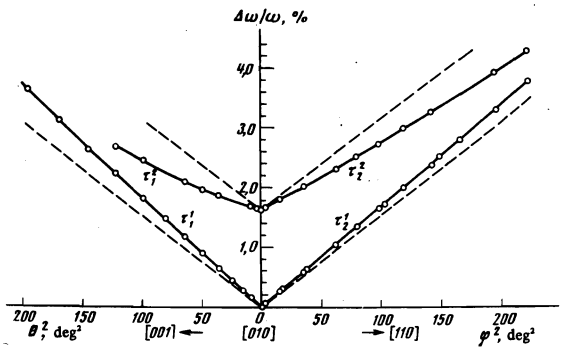

FIG. 6. Angular dependence of the oscillation frequencies τ^1 and τ^2 at small deviations from the [010] axis: right–in (001) plane, left–in (100) plane. Dashed lines–plots of the type $1/\cos\varphi$ and $1/\cos\theta$, which hold for $\partial^2 S/\partial k_z^2 = 0$.

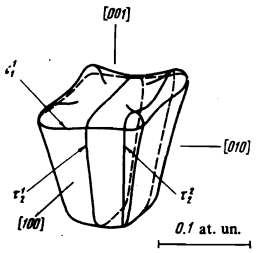

FIG. 7. Electronic part of Fermi surface in zone VI in accord with the data of [7]. Two such volumes are located around the points W of the Brillouin zone [14]. The designations of the sections in this figure and in Fig. 9 below correspond to those in [9,8,7].

squares fit to the functions of Table I with six unknown parameters:

$$\partial \ln S_{1,2}/\partial\sigma_{11}, \quad \partial^2 S_{1,2}/\partial k_z^2, \quad g_{1,2}.$$

During the course of the calculation we also refined the values of the frequencies $\omega_{1,2}$. Table III lists the set of values of all nine parameters that result in the best fit to the functions of Table I. The experimental data were reduced both as a unit and in smaller groups of 510 points each. The difference between the results obtained in this case had made it possible to estimate the errors of the parameters in Table III.

From the angular dependence of the oscillation frequency (Fig. 6) it follows that the branch τ_2^1 pertains to the minimal section of the Fermi surface (Fig. 7), while the branch τ_2^2 pertains to the maximal section. The phase shifts φ_ν of the approximating functions were chosen to take this circumstance into account.

2. u_{33}; **H** ∥ [010]. The measurements of u_{33} were similar to the described measurements of u_{11}. In the pause between these two experiments, the sample was heated, remounted, and again cooled, after which the parameters ${}^{1,2}T_D$ were calculated anew from the field dependence of the oscillation amplitude. From the ratio of the amplitudes of the oscillations u_{33} and u_{11} we calculated the ratios of $\partial \ln S_\nu/\partial\sigma_{33}$ to $\partial \ln S_\nu/\partial\sigma_{11}$. The results of the reduction of the measurements are listed in Table IV. As seen from Tables III and IV, within the limits of the measurement accuracy, the values of ${}^{1,2}T_D$ coincide for these two experiments, and consequently the employed method of mounting the sample [15] does not affect its quality adversely.

3. u_{33}; **H** ∥ [110]. The τ_2^1 oscillations (Figs. 4 and 7) registered at this field direction have an amplitude smaller by a factor ~50 then at **H** ∥ [010]. Since the considered cross section is central, it can be set in correspondence with the effective mass $\mu_6 = 0.377$ [22] measured by the cyclotron-resonance method. The magnetic-interaction parameter is extremely small, $|KA| \sim 10^{-3}$ (T = 0.37 K), so that the analysis of the waveform of the oscillations was not carried out and the values of T_D, g, and $\partial^2 S/\partial k_Z^2$ are not known. Assuming the first two parameters to be isotropic (Tables III and IV), we obtain the estimate

$$|\partial \ln S/\partial\sigma_{ik}|\,|\partial^2 S/\partial k_z^2|^{-1/2} \approx 1.5\cdot 10^{-12}\ \text{cm}^2/\text{dyn}.$$

The small value of this product (and of the amplitude u_{33}) is more readily the consequence of the large curvature $\partial^2 S/\partial k_Z^2 \sim 10^2$ of the cross section passing through the sharp edges of the surface in Fig. 7.

4. u_{11}; **H** ∥ [001]. For this field direction, the oscillations of τ_1^1 (Fig. 7) with frequency $\omega = 28.84 \times 10^6$ rad-G and amplitude $u_{11} = 0.08 \times 10^{-8}$ (H = 8000 Oe, T = 0.37°K) are observed against the background of the δ^1 and δ^2 oscillations that are 20 times stronger (see Item B below). The magnetic interaction for these oscillations is small, $|KA| < 10^{-2}$, and the τ_1^1 oscillations were not taken into account in the analysis of the waveform of the δ-oscillations. The absence of mirror symmetry of the surface in the (001) plane does not make it possible to set the extremal section τ_1^1 in correspondence with any effective mass from among those measured by the cyclotron-resonance method [22]. Using the values $\mu = 0.3$ and $\partial \ln S/\partial\sigma_{11} = 10^5 \times 10^{12}$ cm²/dyn obtained in [6], we can estimate the curvature of the extremal section τ_1^1 at $|\partial^2 S/\partial k_Z^2| \sim 7$.

TABLE III. τ-Oscillations: **H** ∥ [010]

Parameter	Extremal value	
	τ_2^1	τ_2^2
$(\partial \ln S/\partial\sigma_{11})\cdot 10^{11}$, cm²/dyne	+4±0.5	+6.5±1
$g\mu$ *	0.42±0.03	0.73±0.05
	3.58±0.03	3.27±0.05
$\partial^2 S/\partial k_z^{2}$**	0.7±0.2	−6±4
T_D, K	0.09±0.02	0.07±0.02
μ	0.280±0.002	0.331±0.003
μ [22]	0.27	—
$\omega\cdot 10^{-6}$, rad-G	28.073±0.006	28.543±0.006
$\omega\cdot 10^{-6}$ [9]	28.2±0.3	—

*The two possible values of the g factor correspond to the values of the argument $(\pi g\mu/2)$ (4) in the interval from 0 to 2π.

**The errors of the parameters given in the first three lines of the table are determined mainly not by the dispersion but by the correlation of the corresponding quantities. We know with much better accuracy the product.

$$\left(\frac{\partial \ln S}{\partial \sigma_{11}}\right)\cos\left(\frac{\pi}{2}\, g_\nu \mu_\nu\right)\left|\frac{\partial^2 S_\nu}{\partial k_z^2}\right|^{-1/2} = \begin{cases}(3{,}64\pm 0{,}1)\cdot 10^{-11}\ \text{cm}^2/\text{dyne} & (\tau_2^1)\\ (1{,}03\pm 0{,}08)\cdot 10^{-11}\ \text{cm}^2/\text{dyne} & (\tau_2^2)\end{cases}$$

TABLE IV. τ-Oscillations; **H** ∥ [010]

Parameter	Extremal section	
	τ_2^1	τ_2^2
$\frac{\partial \ln S}{\partial\sigma_{33}} / \frac{\partial \ln S}{\partial\sigma_{11}}$	+0.30±0.03	+0.27±0.03
T_D, K	0.06±0.03	0.05±0.02

B. δ-Oscillations; H ∥ [001].

For this direction of the magnetic field, we measured the oscillations of u_{11} (Fig. 8a) at two frequencies with ratio ~1:2. As seen from Fig. 8b, the two groups of oscillations are well resolved at an inclination of 5° to the symmetry axis in the (010) plane. These two frequencies are due to two extremal sections of the hole part of the Fermi surface in zone III (Fig. 9). The results of all the measurements (2550 points u_{11}(H, T = 0.37°K) and 1530 points u_{11}(H, T = 1.28°K)) in

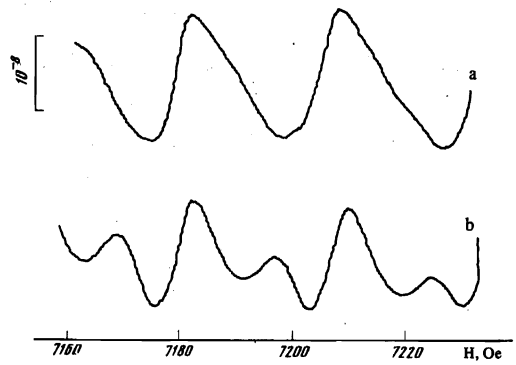

FIG. 8. Waveform of the oscillations of $u_{11}(\delta^1, \delta^2)$ under the conditions T = 0.37 K, $4\pi|\partial M(\delta^1)/\partial H| \approx 0.15$, $4\pi|\partial M(\partial^2)/\partial H| \approx 0.18$: a) at H ∥ [001], b) at ∢ (H, [001]) = 5° in the (010) plane.

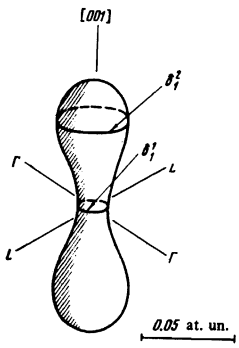

FIG. 9. Hole part of Fermi surface in zone III, according to [9].

the interval H = 4–9 kOe were fed from a punched tape to the computer. The influence of magnetic breakdown, which couples the δ_1^1 orbit with the orbit in band IV, on the oscillation spectrum was considered in Sec. III. The experimental data were approximated by the functions (13) and (15) (Tables II, I). The calculation was performed under the following initial conditions:

1) We used the effective cyclotron masses $\mu(\delta_1^1)$ = 0.10 and $\mu(\delta_1^2)$ = 0.16 measured in [22].

2) Since the three basic functions of the least-squares method, which are derivatives of the sum of the square of the errors minimized with respect to ^1T_D, ^2T_D, and H_3, were not fully orthogonal, i.e., $^\nu T_D$ and H_0 had an appreciable correlation over the system of experimental points, we introduced the same value of T_D for the two cross sections.

3) The curvature of the section δ_1^2 was obtained independently, from data of [7,9], and amounted to

$$\partial^2 S/\partial k_z^2 = -1.94 \pm 0.1.$$

4) The function $\Omega(H)$ [13] in the interval $H_0/H \sim 0.3$–1.3 was approximated, for convenience in calculation, by the relation

$$\Omega = -(0.0514\, H/H_0 - 0.030)^{1/3}.$$

Thus, the approximating functions contained eight unknown parameters:

$$\frac{\partial^2 S_1}{\partial k_z^2}, \quad \frac{\partial \ln S_{1,2}}{\partial \sigma_{11}}, \quad g_{1,2}, \quad T_D, \quad H_0, \quad \frac{\partial \ln H_0}{\partial \sigma_{11}}. \qquad (17)$$

In contrast to Item A of the present section, the field dependence of the amplitude of the oscillations is determined not only by T_D, but also by the last two parameters, so that it is impossible to obtain a preliminary value of T_D prior to the computer calculation. To avoid cumbersome calculations with eight parameters, it is rational to subdivide the set (17) into two weakly-correlated groups, with the first five determining mainly the waveform of the oscillations, and the last three determining the field dependences of the amplitude and phase of the oscillations.

The calculated parameters are listed in Table V. The experimental data at T = 0.37 and 1.28°K were reduced independently, and the errors of the parameters of Table V were estimated from the difference in the results. Figure 10 shows the spectrum of the oscillations of u_{11}, calculated with the parameters of Table V. The spectrum was constructed for H = 7200 Oe and T = 0.37°K, when $4\pi|\partial M_1/\partial H| \sim |K_1^1 A_1| = 0.15$, $|K_1^2 A_1| = 0.18$. Under these conditions, as seen from Fig. 10, the spectral position is determined predominantly by the magnetic interaction and not by the harmonics [2]. From Fig. 10 and Tables I and II it follows that the amplitudes of the lines j = 2, 4, 12, and 13 yield the principal information on the first three parameters of (17)—the amplitude of the lines j = 1 and 24 yield data on the last three parameters, while $g_{1,2}$ are obtained from the ratio of amplitudes of lines j = 1, 2, 3, 6 and j = 24, 12, 13 (owing to the small amplitude of line j = 22).

VI. DISCUSSION OF RESULTS

Using the components of the elastic tensor c_{ijkl}, as calculated by Rayne and Chandrasekhar [23], we can change from derivatives with respect to σ_{lm} to derivatives with respect to the lattice deformation u_{ik}:

$$\frac{\partial}{\partial u_{ik}} = \sum c_{iklm} \frac{\partial}{\partial \sigma_{lm}}. \qquad (18)$$

It is important here that the symmetry group of the undeformed tin lattice [14] contains three sets of mirror planes, and consequently all the first derivatives of S

TABLE V. δ-Oscillations; H ∥ [001]

Parameter	Extremal section δ_1^1	Extremal section δ_1^2
$(\partial \ln S/\partial\sigma_{11}) \cdot 10^{12}$, cm²/dyne	−9.0±0.6	−1.0±0.3
$g\mu$ *	1.62±0.01	1.53±0.02
	2.38±0.01	2.47±0.03
$\partial^2 S/\partial k_z^2$	0.12±0.01	−1.94±0.1
H_0, кэ	7.3	—
$(\partial \ln H_0/\partial\sigma_{11}) \cdot 10^{12}$, cm²/dyne	(1.5±0.3)·10⁴	—
T_D, K	0.28	0.28
$\omega \cdot 10^{-6}$, rad-G	11.0085±0.0010	21.011±0.002
$\omega \cdot 10^{-6}$ [9]	10.8±0.1	20.4±0.2

*See the note in Table III.

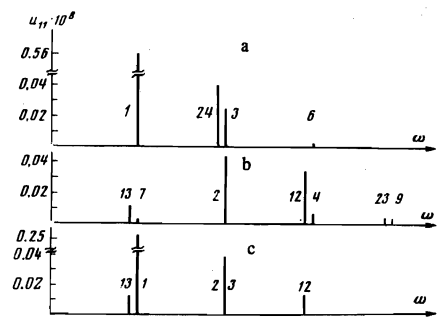

FIG. 10. Spectrum of $u_{11}(\delta^1, \delta^2)$; H = 7200 Oe, T = 0.37°K. a) "Nonrenormalized" spectrum $^I u_{11}$ (13) of the type obtained in [2]; b) new spectral lines of $^I u_{11}$, due to the magnetic interaction; c) strongest lines $^{II} u_{11}$ (15), connected with the magnetic breakdown. The numbers of the lines of the spectrum correspond to the index j in Tables I and II.

and H_0 with respect to u_{ik} with $i \neq k$ vanish. Since the deformation u_{33} does not lift the degeneracy at the point x, it follows that $\partial \ln H_0/\partial u_{33} \ll \partial \ln H_0/\partial u_{11}$, and one measurement of $\partial \ln H_0/\partial \sigma_{11}$ (Table V) is sufficient for the transition (18). For the τ-oscillations, the dependences of $S_{1,2}$ on σ_{11} and σ_{33} (Tables III and IV) form a complete set for the transition (18). For the δ-oscillations, the results of the present paper (Table V) together with the results of direct measurements of the dependence of S on σ_{33} [24] also make up a complete set. To use the data of Perz and Hum [24] we need the components of the tensor $s_{ijkl} = c^{-1}_{ijkl}$. Since the components of this tensor as calculated in [24] from [23] contain some errors, we present their correct values (in units of 10^{-11} cm^2/dyn):

$$s_{11}=0.2296. \quad s_{33}=0.1157. \quad s_{44}=0.3711.$$
$$s_{66}=0.3549. \quad s_{12}=0.1389. \quad s_{13}=0.0281.$$

With these values we obtain from [24]

$$\partial \ln S(\delta^1)/\partial\sigma_{33}=+(22.5\pm2)\cdot10^{-12} \text{ cm}^2/\text{dyn},$$
$$\partial \ln S(\delta^2)/\partial\sigma_{33}=+(4\pm0.4)\cdot10^{-12} \text{ cm}^2/\text{dyn}.$$

In Table VI are summarized the results of the transition (18), and also the derivatives obtained in similar fashion for hydrostatic compression $\sigma_{ik} = -p\delta_{ik}$. These quantities are subject to large errors, since they were obtained by subtracting two large numbers. For comparison, we present the results of direct measurements [3]) of the dependence of the cross section on the hydrostatic compression in the region $p \sim 10^3$—10^4 atm. Measurements of the oscillations of u_{ik} and M [6] in different samples cannot predict the sign, but provide a magnitude estimates

$$\partial \ln S(\delta^1)/\partial p=(-4\text{—}+14)\cdot10^{-12} \text{ cm}^2/\text{dyn},$$
$$\partial \ln S(\delta^2)/\partial p=(-0.8\text{—}+2)\cdot10^{-12} \text{ cm}^2/\text{dyn}.$$

which do not contradict our results (Table VI).

2. The accuracy with which the oscillation frequencies were determined (Tables III and V) was governed by the accuracy with which the magnetic field was measured ($\sim 10^{-4}$), by the accuracy with which it was tied in with the address of the channel ($\sim 10^{-4}$), and by the accuracy with which H was oriented along the symmetry axis of the sample ($\sim 20'$).

The frequencies and effective masses of the τ^1-oscillations obtained in the present study (Table III) agree with the results of measurements by others [9,22]. For the δ-oscillations, there is a discrepancy of $\sim 2\%$ with the results of [9] (see Table V); this is two or three times larger than the measurement error. The ratio $\omega(\delta^2)/\omega(\delta^1) = 1.9078$ agrees with [9] within the limits of errors.

3. The section τ_2^2, $\mathbf{H} \parallel [010]$, passes near the steep edges of the surface shown in Fig. 7, and the value of $\partial^2 S/\partial k_z^2$ for this section is approximately three times larger than for the central section τ_2^1. The amplitude $M(\tau_2^2)$ of the oscillations, according to formula (4) (Sec. II), is attenuated by a factor $|\partial^2 S/\partial k_z^2|^{-1/2}$. In spite of the proximity of the τ_2^1 and τ_2^2 frequencies, their effective masses differ by 20%, so that when the temperature is increased the τ_2^2 oscillations become less noticeable against the background of the τ_2^1 oscillations. These two circumstances seem to explain why the τ_2^2 oscillations were not observed in [8,9] in measurements of the de Haas—van Alphen effect.

TABLE VI

Parameter	Extremal section			
	τ_2^1	τ_2^2	δ_1^1	δ_1^2
$\partial \ln S/\partial u_{11}$	60±8	97±16	−4.9±1.5	−0.04±0.6
$\partial \ln S/\partial u_{33}$	40±6	62±12	+17±2.4	+3.4±0.6
$\partial \ln H_0/\partial u_{11}$	—	—	$+1.8\cdot10^4$	—
$(\partial \ln S/\partial p)\cdot10^{12}$, cm^2/dyn	−92±12	−147±30	−4.5±3	−2±1
$(\partial \ln S/\partial p)\cdot10^{12}$, cm^2/dyne [25]	—	—	−7±0.7	−6.1±0.5

4. The curvature $\partial^2 S/\partial k_z^2$ of the sections of the Fermi surface can be determined after reconstructing the exact shape of the surface by inversion of the experimental data on the anisotropy of the extremal areas. The surface shown in Fig. 9 has a symmetry center, and consequently its shape can be uniquely reconstructed in this manner. The accuracy of the experimental data [8,9], however, is insufficient even to determine the sign of $\partial^2 S/\partial k_z^2$ for the δ_1^1 section. As to the surface shown in Fig. 7, its low symmetry does not make it possible to effect an unambiguous inversion of the experimental data (for example, Fig. 6).

In both cases, nonetheless, we can estimate the curvatures of the sections if we approximate the Fermi surface, at small deviations from the symmetrical directions, by a simple model with one or two parameters. The parameters are determined by comparison with the experimental data on the anisotropy of the cross section or the theoretically available calculations of the Fermi surface.

The results of this estimate, as well as the values of $\partial^2 S/\partial k_z^2$ obtained from the form of the oscillations, are summarized in Table VII. For comparison the table gives also the data obtained from a comparison of the amplitude of the oscillations of u_{ik} [15] with measurements of $\partial \ln S/\partial \sigma_{33}$ [24]. For the surface shown in Fig. 7, we used in the approximation a model that has an additional symmetry element, namely the (001) mirror plane. This model does not take into account the shift of the extremal section with respect to k_z, and consequently leads to an underestimate of $\partial^2 S/\partial k_z^2$. Thus, the data of Table VII are in satisfactory agreement.

5. Performance of the measurements in the range $\Delta H \sim 0.5$ H has made it possible to establish the numbers of the oscillations, i.e., to find the absolute value of the phase. This made it possible to determine the signs of $\partial \ln S/\partial \sigma_{ik}$, while the number of possible values of the g factor satisfying (4) is minimal and is equal to two for each 360° of the argument $(\pi g\mu/2)$ in (4).

TABLE VII

Extremal section	H ∥ axis	$\partial^2 S/\partial k_z^2$	Calculation method*, source of data
δ^1	[001]	$\sim+0.3$	a); [7]
		$\sim+0.5$	a); [8]
		$+0.14\pm0.05$	c); [15], [24]
		$+0.12\pm0.01$	d); Present work
δ^2	[001]	-1.9 ± 0.1	a); [7]
		-2.0 ± 0.2	b); [9]
		~-1.6	a); [8]
τ^1	[010]	$\sim+0.9$	b); [9]
		$\sim+0.12$	b); Present work
		$+0.7\pm0.2$	d); Present work
τ^2	[010]	~-0.4	b); Present work
		-6 ± 4	d); Present work
τ^1	[001]	~-7	c); Present work, [6]
τ^1	[110]	$\sim-(10^2\text{—}10^1)$	c); Present work

*a) Estimate based on results of the calculation of the Fermi surface; b) estimate based on anisotropy of extremal area; c) estimate from measurements of the amplitude u_{ik}, d) determined from the form of the oscillations of u_{ik}.

6. For the δ-oscillations, at $\mathbf{H} \parallel [001]$, $T = 0.37°K$, and $H = 6$ kOe, the parameters of Table V correspond to a magnetic-moment fundamental-frequency amplitude $|^1A_1| \sim 0.1$ G, and $4\pi|\partial M/\partial H|$ reaches a maximum value ≈ 0.3. At these values of KA, all the formulas of Secs. II and III are valid, and the series (13)—(15) converge quite rapidly, as seen from Fig. 1. A sample having this quality (Table V) with a small demagnetizing factor at $T \sim 0.1°K$ should become stratified into diamagnetic domains [14] at those values of the magnetic field $H \sim 10^3$—10^4 Oe, at which

$$4\pi|K_1{}^1A_1+K_2{}^2A_1| \geqslant 1.$$

7. Formula (10) was obtained in [33] for magnetic breakdown between two closed trajectories, i.e., when no open trajectories or two-dimensional grids are produced as a result of the breakdown. In the magnetic-breakdown case considered here (Sec. VB), on the other hand, a two-dimensional open grid of trajectories is produced (Fig. 1), and this should lead to a smearing of the Landau levels into magnetic bands [11]. At $H < H_0$ (the exact estimate depends on the unknown band structure), so long as the band width is much smaller than the distance between the Landau levels of the orbit δ_1^1,

$$\delta\varepsilon \ll \hbar\omega_c, \tag{19}$$

we can classify the bands in accordance with the previous numbers of the levels. The role of the level width T_D will now be played by the field-dependent band width. The accuracy of the experimental data (Sec. VB) is insufficient for a determination of the "true" T_D in the limit of weak fields. Thus, the use of formulas (10) and (11), which ignore the smearing of the levels into bands, to approximate (13) and (15) should overestimate the parameter T_D. This can partly explain the difference, by a factor of 3—4, between the values of T_D for the δ- and τ-oscillations (Tables III—V). Another explanation of this difference is that the orbit δ_1^1 lies near a face of the Brillouin zone (Fig. 1) and is consequently more sensitive to lattice defects.

Since $\hbar k_B^{-1}\omega_c(H_0) \sim 8°K$ and $k_B^{-1}\delta\epsilon \sim T_D \sim 0.3°K$ (Table V), the inequality (19) holds true, and this justifies the use of formula (7).

8. It follows from the value of $\partial \ln H_0/\partial\sigma_{11}$ (Table V) that the breakdown field H_0 should vanish under a uniaxial compression $\sigma_{11} \sim 10^2$ atm. In Fig. 2 this corresponds to the case when the intersection of the two branches of the spectra ϵ_{III} and ϵ_{IV} (dashed lines) occurs at $\epsilon = \epsilon_F$. Instead of an intersection, there should apparently occur a crossover junction between the branches, as shown in Fig. 2b by the solid lines. This "critical" deformation corresponds to a minimal gap ϵ_g^0. It is typical that the effective mass at the limiting point A of the Fermi surface in zone III should change from a value μ_{III} to μ_{IV} on going through this "critical" deformation, where μ_{III} and μ_{IV} are the effective masses at the limiting points of bands III and IV on the XL line in the undeformed lattice. The effective cyclotron mass for the entire orbit δ_1^1, which enters in the amplitude of the oscillatory effects (4), is apparently only insignificantly altered. Thus, the change of $\epsilon_g(\sigma_{11})$ influences the amplitude of the de Haas—van Alphen effect only via the parameter H_0. Since

$$^1A_1 \propto [1-\exp(-H_0/H)],$$

it follows that under critical deformation the amplitude $^1A_1$ of the magnetic-moment oscillations is minimal. The amplitude of the oscillations of the combination frequency [13] under critical deformation will obviously be maximal. Under hydrostatic compression, the lattice symmetry remains unchanged and the effects considered above do not appear.

VII. CONCLUSION

We have shown in this paper that an investigation of quantum oscillations under nonlinear magnetic-interaction conditions makes it possible to obtain additional information from the experiments. Under nonlinear conditions it is possible to measure with an uncalibrated instrument the absolute values of the oscillations of the thermodynamic quantities. This possibility is of fundamental significance in the investigation of magnetostriction. In the present study, the experiment was performed on tin, but it is clear that the magnetic-interaction conditions can be realized in practically all metals [3,11,12]. Thus, the method in question is suitable for all metals and uncovers a possibility of determining, from a single experiment, the following aggregate of quantities: the curvature $\partial^2 S/\partial k_z^2$ of the extremal section of the Fermi surface, its "compressibility" $\partial \ln S/\partial\sigma_{ik}$ (in the case of magnetic breakdown, also the breakdown field H_0 and the derivative with respect to the lattice deformation $\partial \ln H_0/\partial u_{ik}$), the width T_D of the Landau levels, the g factor, the area S of the extremal section of the Fermi surface, and the effective cyclotron mass μ.

With the aid of the existing theoretical calculations of the Fermi surface, we were able to approximate for most metals the experimentally observed anisotropy of the last two quantities, S and μ, with accuracy on the order of several per cent. The extension of the experimental capabilities provides a new set of constants for the energy spectrum of the electrons in the metal, suitable for testing and improving the theoretical calculations of this spectrum.

The authors are grateful to P. L. Kapitza for interest in the work, V. S. Édel'man for help and valuable advice, A. P. Volodin, A. P. Kochkin, I. Ya. Krasnopolin, S. M. Cheremsin for useful discussions, and G. S. Chernyshev for technical help.

[1)] As reported by A. P. Kochkin, it is necessary to correct the sign of Ω in formula (9) of [13].

[2)] This approximation is permissible, since the oscillation amplitude differs from the fundamental-tone amplitude by an amount $\sim (KA)^2 \lesssim 0.01$.

[3)] Table VI lists figures recalculated from the plots of [25] and not from Table I of [25], in which there are errors.

[1] L. D. Landau and E. M. Lifshitz, Teoriya uprugosti (Theory of Elasticity), Fizmatgiz (1965) [Pergamon, 1971].
[2] I. M. Lifshitz and A. M. Kosevich, Zh. Eksp. Teor. Fiz. **29**, 730 (1955) [Sov. Phys.-JETP **2**, 636 (1956)].
[3] R. A. Phillips and A. V. Gold, Phys. Rev. **178**, 932, 1969.
[4] D. Shoenberg and J. Vanderkoy, J. Low Temp. Phys. **2**, 484, 1970.
[5] R. Griessen and R. Sorbello, Phys. Lett. **38A**, 353, 1972.
[6] M. M. Finkelstein, J. Low Temp. Phys. **14**, 287, 1974.
[7] J. E. Craven, Phys. Rev. **182**, 693, 1969.
[8] M. D. Stafleu and A. R. de Vroomen, Phys. St. Sol. **23**, 675, 1967.
[9] J. E. Craven and R. W. Stark, Phys. Rev. **168**, 849, 1968.

[10] M. M. M. P. Matthey and A. R. de Vroomen, Solid St. Com., 9, 1329, 1971.
[11] A. Pippard, transl. in: Fizika metallov (Metal Physics), Vol. 1, Mir, 1972.
[12] D. Shoenberg, Canadian J. Phys. 46, 1915, 1968.
[13] A. P. Kochkin, Zh. Eksp. Teor. Fiz. 54, 603 (1968) [Sov. Phys.-JETP 27, 324 (1968)].
[14] S. Mase, J. Phys. Soc. Japan 14, 1538, 1959.
[15] V. M. Pudalov and M. S. Khaĭkin, ZhETF Pis. Red. 15, 14 (1972) [JETP Lett. 15, 9 (1972)].
[16] V. M. Pudalov, ZhETF Pis. Red. 19, 466 (1974) [JETP Lett. 19, 250 (1974)].
[17] M. S. Khaĭkin, S. M. Cheremisin, and V. S. Édel'man, Prib. Tekh. Eksp., No. 4, 225 (1970).
[18] V. M. Pudalov and M. S. Khaĭkin, Prib. Tekh. Eksp., No. 6, 218 (1968).
[19] M. S. Khaĭkin, Prib. Tekh. Eksp., No. 3, 104 (1961).
[20] V. P. Zelenin, G. G. Kudymov, Yu. G. Svetlov, and V. A. Troshev, Prib. Tekh. Eksp., No. 1, 229 (1969).
[21] V. P. Zelenin, V. M. Pudalov, Yu. G. Svetlov, and A. G. Mikhailovskii, Prib. Tekh. Eksp., No. 2, 130 (1972).
[22] M. S. Khaĭkin, Zh. Eksp. Teor. Fiz. 42, 27 (1962) [Sov. Phys.-JETP 15, 18 (1962)].
[23] J. A. Rayne and B. S. Chandrasekhar, Phys. Rev. 120, 1658, 1960.
[24] J. M. Perz and R. H. Hum, Canadian J. Phys. 49, 1, 1971.
[25] N. B. Brandt, S. V. Kuvshinnikov, and Ya. G. Ponomarev
[24] J. M. Perz and R. H. Hum, Canadian J. Phys. 49, 1, 1971.
[25] N. B. Brandt, S. V. Kuvshinnikov, and Ya. G. Ponomarev, ZhETF Pis. Red. 19, 201 (1974) [JETP Lett. 19, 123 (1974)].

Translated by J. G. Adashko
240